HURRICANE - GENERATED OCEAN WAVES

Fumin Xu[1,2], Will Perrie [1] Bechara Toulany[1] and Peter C. Smith[1]

[1]Fisheries and Oceans Canada, Bedford Institute of Oceanography, Dartmouth, NS, Canada
[2]College of Ocean Engineering, Hohai University, Nanjing, P. R. China
Email: xuf@dfo-mpo.gc.ca

1. INTRODUCTION

Juan reached hurricane strength at 1200 UTC 26 Sept. near Bermuda, as it moved towards Nova Scotia with increasing propagation speed (Fogarty et al., 2006; http://projects.novaweather.net/work.html). At its peak, maximum winds were 90 knots at 1800 UTC 27 Sept. when it was north of the Gulf Stream. Soon afterwards, it intensity began to weaken by 1800 UTC 28 Sept., as its translation speed continued to accelerate, typical of extratropical hurricanes. Juan made landfall near Halifax (0300 UTC 29 Sept.), with winds of 85 knots. Table 1 gives detailed storm characteristics and best track estimates (Avila, 2004) from 0300 UTC 27 Sept. to 0900 UTC 29 Sept. Figure 1 shows the dramatic increase in Juan's translation speed during this period, from 2.28m/s to 20m/s.

In this paper, we present analyses of observed wave data in Section 2 and wave model simulations in section 3. Shallow water waves are discussed in section 4, including two-dimensional (2D) wave spectra. Section 5 discusses simulation results; and section 6 gives conclusions.

Table 1. Hurricane Juan Characteristics.
Time is indicated as hour UTC / day in Sept. 2003, mean sea level pressure (hPa) is denoted SLP, diameter of the eye (nm) is indicated 'eye', and maximum sustained winds (kt) is indicated 'U_{10}'.

time	Position		SLP	eye	U_{10}	Radius(nm)											
	Lon. (°W)	Lat. (°N)				34kt				50kt				64kt			
						NE	SE	SW	NW	NE	SE	SW	NW	NE	SE	SW	NW
03/27	61.9	33.7	984		70	175	100	50	120	30	30	30	30	20	20	20	20
09/27	62.4	34.9	981	15	75	175	100	60	120	40	40	40	40	20	20	20	20
15/27	63.0	35.3	979	15	75	175	100	60	120	40	40	30	40	20	20	20	20
21/27	63.4	35.9	970	20	90	175	120	60	120	40	40	30	40	25	25	25	25
03/28	63.8	36.8	970		90	175	120	50	120	50	50	50	50	30	30	30	30
09/28	64.1	37.6	970	15	90	175	120	80	120	50	50	50	50	30	30	30	30
15/28	64.1	39.4	973		85	200	150	100	200	60	60	60	60	60	30	30	30
21/28	64.1	41.2	973		85	200	150	100	120	60	60	60	60	60	30	30	30
03/29	63.8	44.5	974		70	150	100	100	100	60	60	60	60	60	30	30	30
09/29	63.4	47.8	987		60	150	150	100	150	80	80	40	40				

2.WAVE OBSERVATIONS

Figure 2(a) shows Juan's wind swath isolines and six buoy locations (Table 2) within or near the 10m/s wind swath isoline: buoys 44140, 44008, 44018 and 44011 are in intermediate water depth, whereas buoys 44142 and 44137 are in deep water. While buoy 44142 is on the storm track, buoy 44137 is on the right side of the storm track, outside the maximum wind radius.

Figures 3(a)~3(b) give observed one-dimensional (1D) frequency wave spectra time series at buoys 44137 and 44142. Data from the other buoys are presented at the Workshop. Swell-domination and its interactions with wind-wave spectra are important components of the overall wave spectra at most of these buoys. For example, in terms of swell dominating spectra and wind-wave spectra, Juan had slight influence on data from buoy 44140, although it strongly influenced buoys 44008 and 44018. These three buoys are all on the 10m/s wind swath isoline. At buoy 44011, swell-domination existed over 24 hours. At buoy 44142, extremely low frequency strong swell appeared around 0000 UTC 29 Sept. and lasted for about two hours, during the time of peak waves. At buoy 44137, swell existed over 24 hours, until peak waves developed at 0000 UTC 29 Sept., continuing for about 3 more hours.

Therefore, in areas along the track and on the left of the track, swell domination over wind waves extended over a period of almost over 24 hours, before, during and after Juan's passage by the buoys. During the time when Juan's wind fields have influence, waves at different buoy locations show totally different behaviours in strength, duration and spectral pattern.

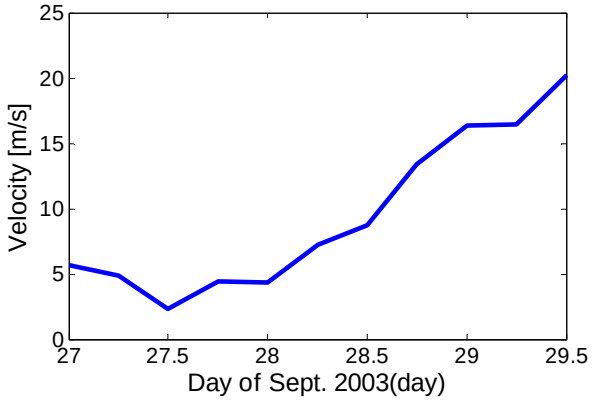

Figure 1. Translation speed for hurricane Juan.

Table 2 Buoy observation locations.
Buoys 44008, 44018, 44011 and 44140 are maintained by the US National Data Buoy Center, whereas 44140, 44142, and 44137 are maintained by Environment Canada. Position is in degrees (latitude, longitude).

Buoy station	44008	44018	44011	44140	44142	44137
Position	(40.50, 69.43)	(41.26, 69.29)	(41.11, 66.58)	(43.75, 51.74)	(42.50, 64.02)	(42.26, 62.0)
Water depth	62.5m	74.4m	88.4m	90m	1300m	4500m

3. WAVE MODEL SIMULATIONS

WAVEWATCH III (Tolman, 2002), hereafter denoted WW3, is used on a coarse domain (75º W~40ºW, 20ºN~65ºN), shown in Figure 2, with 15' space resolution. COAMPS (FNMOC Monterey) wind fields are used for Juan's outer region. Winds for the central core region of the storms ($14.4^o \times 7.2^o$ centered on the hurricane's 'best track'), are defined by a new blending interpolation method developed by Xu et al. (2006).

Figures 2(b)~2(c) give WW3-simulated significant wave height (Hs) and average wave length (L) swath maps. It is clear that the Hs and especially the L swath distributions are more asymmetric than Juan's wind swath distribution. Moreover, hurricane-generated waves can cover a far larger area than the associated storm winds, because swell waves can extend over the ocean. Maximum Hs values appear just to the right side of the storm track, whereas notably larger and more complex structures for L values occur on the left side of the track than on the right side. Swell dominates, and propagates outside of Juan's wind range on the left side of the track. On the right side of Juan's track, less swell is evident, even within the 10m/s wind swath isoline. Storm translation speed is also a consideration. Strong swell appears on the right side of the track only when translation speed approximates or surpasses the dominant wave group velocity, as shown in Figure 2(c).

4. WAVES IN SHALLOW WATER

4.1 OBSERVATIONS (WINDS AND WAVES)

Within the Lunenburg Bay (denoted "the Bay"), five observation stations are available, as indicated by symbols DWR, ADCP, MB1, SB2 and SB3 (in Figure 4). Wind observations are available at the SB2, SB3 and MB1 locations. As these three locations are near land, they experience some sheltering effects. Hence, the actual winds at the DWR and ADCP locations tend to be slightly larger than those estimated from the 3

nearshore sites. Two-dimensional spectral wave observations are recorded by the DWR and ADCP.

For Lunenburg Bay domain (Figure 4), observed winds at the SB2, SB3 and MB1 stations are used to define the driving wind fields, as shown in Figure 5. To compensate for the change in surface roughness in going from land to water, the wind field is increased by a factor of 1.25 (Perrie and Toulany, 1990, Fig. 1).

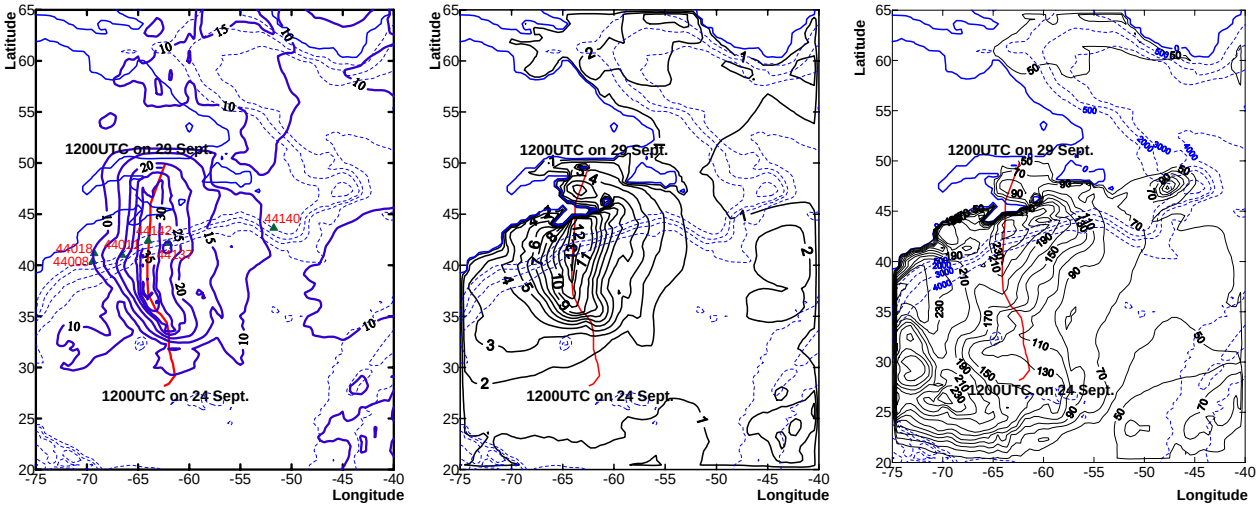

Figure 2. Computational domain showing Juan's track (red contour ——), four dashed contour lines representing 500, 2000, 3000, and 4000 m bathymetry isolines at the continental shelf-break, and: (a) wind velocity swath isolines (units in ms^{-1}**)**, (b) WW3 simulated significant height (Hs) swath isolines (units in m), and (c) WW3 simulated average wave length (L) swath map (units in m**)**.

4.2 MODEL DOMAIN AND RESOLUTION

The SWAN (Booij et al., 1996) model and a high resolution domain is used for the Bay (see Figure 4). We use a spatial resolution of 60m on the domain (64.35°W ~ 64.17°W, 44.28°N ~ 44.38°N). As the Bay is located on the left side of Juan's track, swell dominates the wind-waves of this region for over 24 hours, before, during and after Juan's passage (sections 2 and 3). Computational spectral resolutions match the observed spectral resolutions: directional resolution is 4°, the computational frequency domain range from 0.04Hz to 0.58Hz, with neighbouring frequencies defined as $f = 1.0434\, f_n$.

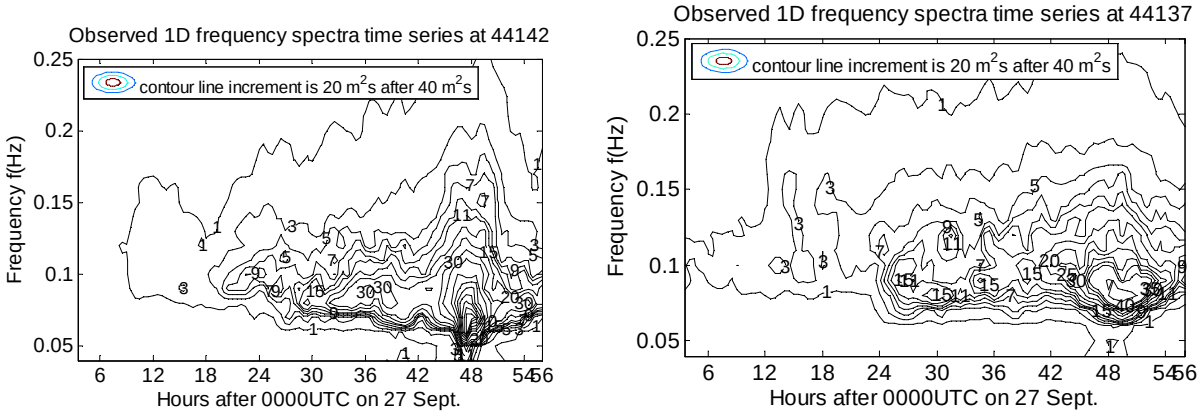

Figure 3. Observed 1D frequency spectra time series at buoys 44142 and 44137.

4.3 BOUNDARY CONDITIONS

Boundary conditions are always a problem. Only 1 observation point (DWR) is available near the lower east boundary of the Bay grid, as shown in Figure 4, with 2D observed spectra recorded every half hour. With different water depths, positions and topography, waves along the open boundaries of the Bay (the east and south boundaries), have differing directions and spectral densities, as a function of time.

To solve this problem, a larger domain including Mahone Bay is used (Figure 6), which is nested within a fine-resolution domain (65ºW~63ºW, 43ºN~45ºN), in turn nested within an intermediate-resolution domain (71º W~55ºW, 42ºN~62ºN), which is nested within the coarse-resolution domain (section 3). Resolutions in the 4 domains are 130m, 1', 5', and 15', respectively. Directional resolution is 6°. Frequencies range from 0.03094Hz to 0.5939Hz, with neighbouring frequencies defined as $f = 1.1\, f_n$. Blended winds (Xu, et al. 2006) are applied in these domains (section 3). WW3 is used on the coarse and intermediate domains; SWAN is used on the fine and very-fine (Mahone Bay) domains.

From the Mahone Bay domain computation, values for correlations between waves at open boundary points (Figure 6) and at the DWR are obtained, by constructing relationships between significant wave heights (Hs) and average wave directions (DIR). Results show that DIR at all these points and DWR are almost the same, while Hs values vary, as shown in Table 3.

We assume that the 2D wave spectra have similar spectral shapes at each grid point on the east and south boundaries and at the DWR location, because these spectra experience almost the same winds and same propagating swell. Therefore, 2D spectra at open boundary points of the Bay are obtained by: $S_p(f,\theta) = \kappa^2 S_{DWR}(f,\theta)$, where κ is the ratio of Hs at open boundary points to Hs at DWR (Table 3).

Table 3 Hs Relationship between open boundary points of Lunenburg Bay and DWR, where longitude and latitude are indicated as well as the ratio, $\kappa = Hs / Hs_{DWR}$, P1, P2, …, P16 are shown in Fig.6, along the Lunenburg Bay open boundaries, in counter clockwise order.

Points	P1	P2	P3	P4	P5	P6	P7	P8	P9	P10	P11	P12	P13	P14	P15	P16
Longitude	64.24	64.23	64.22	64.21	64.20	64.19	64.18	64.17	64.17	64.17	64.17	64.17	64.17	64.17	64.17	64.17
Latitude	44.28	44.28	44.28	44.28	44.28	44.28	44.28	44.29	44.30	44.31	44.32	44.33	44.34	44.35	44.36	44.37
γ	0.85	0.92	0.90	0.93	0.97	1.01	1.02	1.02	1.07	0.90	0.85	0.86	0.89	0.85	0.81	0.80

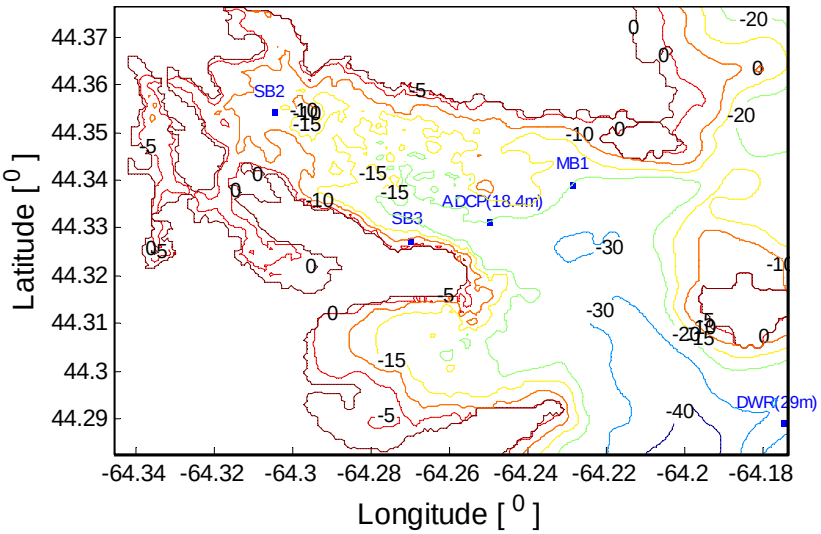

Figure 4 Lunenburg Bay computation domain, observation points DWR, ADCP, MB1, SB2 and SB3.

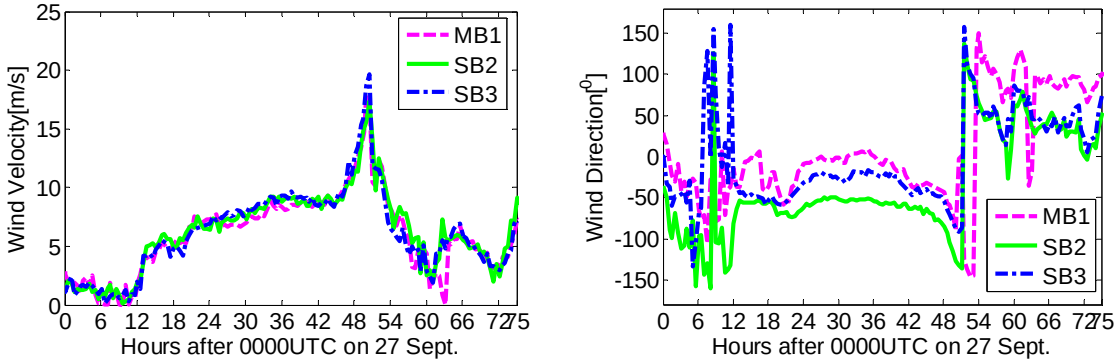

Figure 5 Observations at SB2, SB3 and MB1: (a) wind velocity and (b) wind directions.

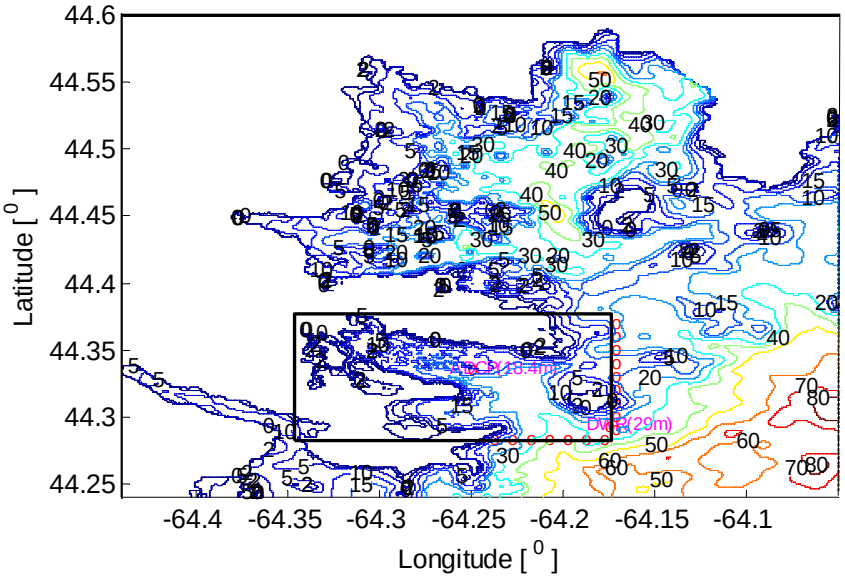

Figure 6 Mahone Bay computational domain, Lunenburg Bay domain, open boundary points of the Lunenburg Bay domain, and observation points (ADCP and DWR).

5. SIMULATION RESULTS

In the Lunenburg Bay domain, the winds and the incoming 2D spectral open boundary conditions are relatively accurate, and thus we expect accurate simulation results, assuming accurate model physics.

Prescribed JONSWAP-shape 2D spectra are also used as open boundary conditions, based on the observed Hs, Tp, and PDIR, to test the influence of input boundary spectral shape on the simulation results (with JONSWAP spectral peak enhancement parameter set to 7 and directional spreading factor, 8, to describe the incoming swell). Model physics are customized for the Lunenburg Bay implementation: for wind input, whitecapping and nonlinear wave-wave interactions (triad and quadruplet), default settings are applied; for bottom friction, $C_{bottom} = 0.038 m^2 s^{-3}$ is used; for depth-induced breaking, we suggest that the narrow low-frequency and narrow directional band of dominant swell doesn't break. This will be discussed in detail in the future paper, and here, depth-induced breaking is not used.

Figure 7a~7b are simulations of Hs and Tp at the ADCP location, compared with observations.

6. SUMMARY AND ANALYSES

Hurricane Juan was one of the most damaging storms in the modern history of Nova Scotia. Observations and the wave model simulations show that: (1) the range influenced by hurricane-generated waves is far larger than the wind vortex range; (2) swell dominates on the left side of the track, the track and the right side near the track, before, during and after Juan's passage, and also that the Juan-induced waves zone on the left of the track is larger than that on the right side, although the largest waves occur near the track on the right side; (3)

different locations within Juan's vortex show totally different waves strength and spectral pattern.

To ensure accurate boundary conditions for the simulation of waves in Lunenburg Bay, the open boundary conditions were resolved by constructing detailed relationships between 2D wave spectra at open boundary points and those at the DWR location, through nesting the Mahone Bay domain within a series of larger domains.

With accurate observed driving wind fields and 2D spectra boundary conditions, simulated Hs and Tp compare better with ADCP data than those that assume prescribed JONSWAP 2D boundary spectra, especially the peak period Tp, which suggests that the dominant swell is therefore simulated reasonably. However, at the ADCP, the simulated Hs is still lower than the wave observations, during peak waves, and a little higher than observations before and after peak waves.

Several factors contribute to the results that we have obtained: (1) The DIA formulation is used for quadruplet nonlinear wave-wave interactions, in which the frequency increment factor is assumed: $\gamma = 1.1$, while $\gamma = 1.0434$ is applied in Lunenburg Bay, to ensure enough spectra resolution for extremely narrow band swell. The deviation of γ biases more energy transfer to lower frequencies. We have compared the quadruplet nonlinear wave-wave interactions from DIA and WRT (Webb-Resio-Tracy Method), under Juan-generated wind waves, swell dominant and wind waves plus swell conditions. Details will be described in future paper. (2) We did not use depth-induced breaking during simulation, which results in better results during peak waves and slight overestimations before and after peak waves. (3) Currents from tides, wind, storm surge and waves combine to influence the waves, and need to be taken simulated. (4) JONSWAP parameterizations of 2D spectra are not adequate to describe the extremely narrow frequency and directional band swell spectra. (5) Simulations of peak waves need further research, to be presented in a future papers. (6) As well as shallow water areas within Lunenburg Bay, questions remain regarding the SWAN model behaviour, in such shallow water with extremely narrow spectral band swell waves. (7) Biases in ADCP wave measurements are a problem.

Acknowledgments

Support is from the Canadian Panel on Energy Research and Development, the China Scholarship Council, GoMOOS - the Gulf of Maine Ocean Observing System, CFCAS (Canada Foundation for Climate and Atmospheric Studies), and SCOOP, the Southeast Universities Research Association Coastal Ocean Observing and Prediction program.

REFERENCES

Avila, L.A, 2004: Hurricane Juan 24-29 September 2003. NOAA National Hurricane Center/ TPC. [http://www.nhc.noaa.gov/2003Juan.shtml].

Booij, N., Holthuijsen, L.H. and Ris, R.C., 1996: The "SWAN" Wave Model For Shallow Water, *Coastal Engineering*, **1**, 68~672.

Fogarty, C. T., Greatbatch, R. J., and Harold, H., 2006: The role of anomalously warm sea surface temperatures on the intensity of Hurricane Juan (2003) during its approach to Nova Scotia. In press, in *Monthly Weather Rev*.

Tolman, H. L., 2002: User manual and system documentation of WAVEWATCH-III version 2.22. Online at http://polar.ncep.noaa.gov/waves.

Xu, F., Perrie, W., Toulany, B., and Smith, P. C., 2006: Wind-generated waves in Hurricane Juan. Submitted to Ocean Modelling.

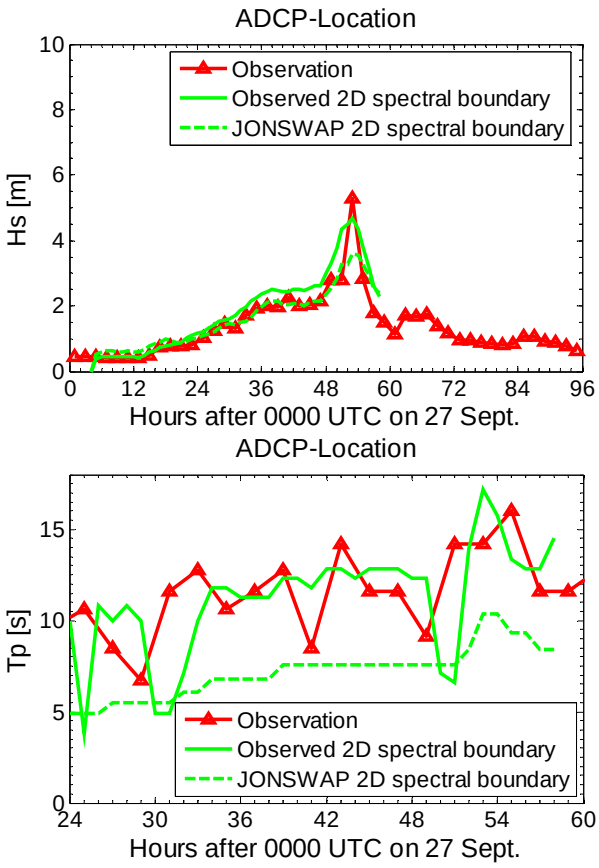

Figure 7. Simulated Hs and Tp at ADCP, compared with observations.